

EQ1 ► INVITED SUBMISSION

 AU1 ► **Biomaterialized Recombinant Collagen-Based Scaffold
Mimicking Native Bone Enhances Mesenchymal
Stem Cell Interaction and Differentiation**

 AU3 ► AU2 ► Gloria Belén Ramírez-Rodríguez, Monica Montesi, Silvia Panseri, Simone Sprio,
Anna Tampieri, and Monica Sandri

The need of synthetic bone grafts that recreate from macro- to nanoscale level the biochemical and biophysical cues of bone extracellular matrix has been a major driving force for the development of new generation of biomaterials. In this study, synthetic bone substitutes have been synthesized via biomimetic mineralization of a recombinant collagen type I-derived peptide (RCP), enriched in tri-amino acid sequence arginine–glycine–aspartate (RGD). Three-dimensional (3D) isotropic porous scaffolds of three different compositions are developed by freeze-drying: **nonmineralized** (RCP, as a control), mineralized (Ap/RCP), and mineralized scaffolds in the presence of magnesium (MgAp/RCP) that closely imitate bone composition. The effect of mineral phase on scaffold pore size, porosity, and permeability, as well as on their *in vitro* kinetic degradation, is evaluated. The ultimate goal is to investigate how chemical (i.e., surface chemistry and ion release from scaffold) together with physical signals (i.e., surface nanotopography) conferred via biomimetic mineralization can persuade and guide mesenchymal stem cell (MSC) interaction and fate. The three scaffold compositions showed optimum pore size and porosity for osteoconduction, without significant differences between them. The degradation tests confirmed that MgAp/RCP scaffolds presented higher reactivity under physiological condition compared to Ap/RCP ones. The *in vitro* study revealed an enhanced cell growth and proliferation on MgAp/RCP scaffolds at day 7, 14, and 21. Furthermore, MgAp/RCP scaffolds potentially promoted cell migration through the inner areas reaching the bottom of the scaffold after 14 days. MSCs cultured on MgAp/RCP scaffolds displayed higher gene and protein expressions of osteogenic markers when comparing them with the results of those MSCs grown on RCP or Ap/RCP scaffolds. This work highlights that mineralization of recombinant collagen mimicking bone mineral composition and morphology is a versatile approach to design smart scaffold interface in a 3D model guiding MSC fate.

 AU5 ► **Keywords:** biomimetic mineralization, magnesium, mesenchymal stem cell, osteogenic differentiation, recombinant collagen, scaffold

Introduction

 AU6 ► **B**ONE IS A dynamic tissue in continuous process of formation, growth, and remodeling with the capacity to repair itself and heal fracture below a critical size defect.¹ Nevertheless, some pathological conditions such as large traumatic injury, degenerative diseases, tumor or bone fragility related to aging of the population are still a major challenge in common clinical practice requiring the use of bone grafts to support and stimulate the formation of new bone.² In fact, the demand of bone substitutes is expected to steadily increase worldwide in the next decades due to the lengthening life expectancy.³ Several types of bone graft, such as autograft (i.e., patient bone), allograft (i.e., bone

 from donor), xenograft (i.e., bone from animal source), and synthetic bone grafts (e.g., metal, ceramic, polymers, or composite materials) are available to repair/substitute the bone defects.⁴ However, current bone substitutes present certain drawbacks. On one hand, the use of autografts is limited due to donor-site morbidity and shortage of supply, whereas allografts and xenografts exhibit the risk of immune rejection in host body and transmission of viral diseases and bacterial infection.⁵ On the other hand, and despite the progress on tissue engineering, synthetic bone grafts still have unsatisfactory outcomes mainly related to low rate of biodegradability, lack of mechanical features, and inadequate biological, chemical, and/or architectural properties that reduce biomaterial–host tissue interaction.⁶

AU4 ► Institute of Science and Technology for Ceramics (ISTEC), National Research Council (CNR), Faenza, Italy.

Since the cells in tissues adhere to and interact with their extracellular environment via specialized cell–cell and cell–extracellular matrix (ECM) contacts, the ideal scaffolds should mimic the natural ECM of the host tissue as much as possible. Langer and Vacanti⁷ underlined the requirement of design of scaffolds with sufficiently interconnected pores of appropriate size to facilitate vascularization and simultaneously modulating the material surface biochemistry and nano/microscale surface topographies, to formulate favorable binding sites to actively regulate and control cell and tissue behavior, while interacting with host cells. Native bone consists in a homogeneous hybrid matrix made of self-assembled collagen fibrils reinforced by inter- and intrafibrillar crystallization of nonstoichiometric hydroxyapatite containing foreign ions into its structure (i.e., Mg, Sr, Na, CO₃).⁸ The design of nanocomposites, recapitulating the organization of natural bone ECM, has certainly constituted a major breakthrough in bone tissue engineering.⁹ Organic macromolecules such as natural polymers (i.e., including collagen, cellulose, chitosan, gelatin, alginate, and fibroin) have been used as template/matrix to develop nanocomposite scaffolds via biomimetic mineralization.^{10–14} Recent research in the tissue engineering field has involved the use of synthetic peptide engineered with biological function of native ECM proteins.¹⁵ The design of bone-like scaffolds moves toward the biomimetic mineralization of synthetic peptides and proteins combining the possibility to engineer synthetic peptide sequences with specific biofunctionality with the chance to tailor the physicochemical properties of the mineral phase via controlled biomineralization processes. Several studies on the mineralization of recombinant human-like collagen have been carried out as potential biomaterial for bone regeneration.^{16–18} In this line, our group has investigated the bioinspired mineralization of recombinant collagen type I-derived peptide (RCP).¹⁹ RCP (commercialized under the trade name of Cellnest™) is based on human collagen type I (α I chain) and enriched with arginine–glycine–aspartate (RGD) sequences, the cell attachment site of a large number of adhesive ECM, blood, and cell surface proteins.²⁰ RCP is proposed as a promising biomaterial in regenerative medicine thanks to versatile formulation and applications.^{21,22} Nevertheless, engineering of three-dimensional (3D) scaffold through biomimetic mineralization of synthetic peptides to ensure mesenchymal stem cell (MSC) adhesion, migration, and their differentiation to osteogenic lineage still remains in its infancy.

Herein, the objective of the present work is to design bioactive, biofunctional, and biodegradable scaffolds for bone tissue regeneration through biomimetic mineralization of RCP. The effect of mineral phase on scaffold pore size, porosity, and permeability, as well as on their *in vitro* kinetic degradation, is evaluated. The ultimate point is the investigation of the *in vitro* response of MSCs to the biochemical and biophysical cues provided to the scaffolds by biomimetic mineralization.

Materials and Methods

Scaffold preparation

Three-dimensional isotropic porous scaffolds of three different compositions are developed: nonmineralized scaffolds (RCP, as a control), mineralized scaffolds (Ap/RCP), and

mineralized scaffolds in the presence of magnesium (MgAp/RCP) that closely mimic bone apatite composition (Mg \approx 0.5–1 wt. %).²³ Nanocomposite 3D scaffolds were synthesized by biomimetic mineralization of RCP (kindly supplied by Fujifilm Manufacturing Europe BV) for an initial theoretical mineral/organic weight ratio of 40/60, as described in our previous work.¹⁹ Briefly, it started with the dissolution (at 40°C) of RCP (1.5 mM) into 5 mL of phosphoric acid (H₃PO₄, purity \geq 85 wt. %) aqueous solution (0.71 M). The resulting RCP/H₃PO₄ solution was added dropwise to a calcium hydroxide [Ca(OH)₂, purity \geq 95%] suspension (1.18 M) in 5 mL of water (Ca/P molar ratio of 1.67) and vigorously stirring at room temperature for 2 h. RCP mineralization was also carried out in the presence of magnesium chloride hexahydrate (MgCl₂·6H₂O, \geq 99% purity) by adding it to Ca(OH)₂ suspension (initial Mg/Ca molar ratio of 0.15). The final solution pH was 10 in both cases. The mineralized suspension was poured into a 12-well plate (4 g per well) and freezer at –20°C overnight. The material was freeze-dried with a heating ramp of 5°C/h under vacuum (0.1 mbar; 5 Pascal; Cinquepascal srl). Non-mineralized scaffolds (RCP) were prepared as a control by freeze-drying RCP aqueous solution (7.5 wt. %). Cylindrical scaffolds of 8 mm in diameter and 5 mm of height were obtained by cutting with a biopsy puncher (HS biopsy punch 8 mm; HS Hospital Service).

Then, scaffold stability and degradability rate were adjusted by physical crosslinking via dehydrothermal treatment at 160°C for 48 h under vacuum.²² All scaffolds were sterilized by autoclave before *in vitro* degradation studies and cell culture.

Characterization of the physicochemical properties of designed scaffolds

X-ray diffraction (XRD) patterns of the scaffolds were recorded on a D8 Advance diffractometer (Bruker, Karlsruhe, Germany) equipped with a Lynx-eye position sensitive detector using Cu K α radiation (λ = 1.54178 Å) generated at 40 kV and 40 mA. Spectra were recorded in the 2θ range from 10° to 60° with a step size (2θ) of 0.02° and a counting time of 0.5 s. Fourier transform infrared (FTIR) spectroscopy analyses were carried out on a Nicolet 5700 spectrometer (Thermo Fisher Scientific, Inc., Waltham, MA) with a resolution of 2 cm⁻¹ by accumulation of 64 scans covering the 4000–400 cm⁻¹ range, using the KBr pellet method. Inductively coupled plasma optical emission spectrometry (ICP-OES; Agilent Technologies 5100 ICP-OES, Santa Clara, CA) was used to analyze the chemical composition (Ca, P, and Mg) of mineralized scaffolds (Ap/RCP and MgAp/RCP). For this purpose, 20 mg of scaffold was dissolved in 2 mL of ultrapure nitric acid and then diluted up to 100 mL. Three replicates were prepared for each condition. Then, dilute solutions were analyzed for analytical emission wavelengths: Ca (422 nm), Mg (279 nm), and P (214 nm).

Scanning electron microscopy (SEM; ESEM FEI Quanta 200) was used to analyze the intrinsic morphology of the scaffolds. Transversal and longitudinal scaffold sections were fixed on aluminum stubs using a carbon tape and sputtered with a 20-nm-thick gold layer. SEM images were acquired at 10 KeV at high vacuum. The mean pore size of RCP, Ap/RCP, and MgAp/RCP scaffolds was obtained by

measuring 60 pores from SEM micrographs with ImageJ software (version 1.48v; NIH, Bethesda, MD). Total porosity was measured by gravimetry according to the following equation:

$$\%porosity = 100 \times [1 - (\rho_{scaffold} / \rho_{material})] \quad (1)$$

where $\rho_{material}$ is the density of the material of which the scaffold is fabricated and $\rho_{scaffold}$ is the apparent density of the scaffold measured by dividing the weight by the volume of the scaffold.²⁴ Density of RCP is considered 1.3 g/cm³ according to technical specification, and apatite density is considered 3.16 g/cm³ according to the literature.²⁵

The scaffold permeability was evaluated by falling head method. It consists in measuring the time that a fluid column drops from the upper (H_1) to the lower level (H_2) of a standpipe while fluid flows through the scaffold, which is hosted to a permeability chamber that is directly connected to the standpipe. Five scaffolds per condition were autoclaved in phosphate-buffered saline (PBS) and maintained in PBS solution overnight (37°C) before the measurements. The scaffold permeability constant was calculated according to Darcy's law²⁶:

$$k = \frac{aL}{A} \frac{\mu}{t \rho g} \ln \frac{H_1}{H_2} \quad (2)$$

where k is scaffold permeability (m²); a , cross-sectional area of standpipe (mm²) $a = \pi r_p^2$; A , cross-sectional area of scaffold (mm²) $A = \pi r_s^2$; L , scaffold thickness (m); t , time for PBS going from H_1 to H_2 (s); H_1 , H_2 , height of PBS column (cm); μ , dynamic viscosity of fluid (Nsm⁻²); ρ , density of fluid (kg/m³); and g , gravity (m/s²).

Evaluation of in vitro degradation of scaffold

The physiological stability and degradability of the scaffolds were evaluated by measuring the total weight loss of the scaffolds as well as the ion release from the mineral phase and the RCP release from organic matrix. Briefly, three scaffolds (30 mg) per group and time point were immersed in 10 mL of PBS solution (pH=7.4) at 37°C over the course of 4 weeks. At scheduled time points (7, 14, 21, and 28 days), three scaffolds were removed from the liquid, rinsed with Milli-Q water, dried in an oven at 40°C overnight, and weighted (W_i). The percentage of the weight loss was calculated as follows:

$$Weight\ Loss\ (\%) = 100 \cdot (W_i - W_f) / W_i \quad (3)$$

where W_i is the starting dry weight before immersion into PBS solution.

At each time point, PBS was collected and refreshed with a new one. The collected PBS medium was used to determine the ion release as well as the RCP release to the medium. For ion release studies, PBS medium was filtered, treated with nitric acid, and diluted in Milli-Q water for evaluation of element concentration (Ca and Mg) by ICP-OES. The ion release is represented as weight percentage of Ca-Mg release with respect to the total Ca-Mg content in the scaffold. For determination of RCP release, PBS medium was centrifuged at 4500 g for 15 min at 4°C, and protein

concentration of the supernatant was calculated by a colorimetric assay (Kit DC Protein Assay; Bio-Rad). The RCP release is represented as weight percentage with respect to the total weight of the scaffold. **Data are expressed as average \pm standard error of the mean (SEM; $n=3$).**

Cell culture and cell seeding on scaffolds

Mouse MSCs (C57BL/6), purchased from Invitrogen (Carlsbad, CA), were cultured in standard tissue culture flask and maintained in standard cell culture Dulbecco's modified Eagle's medium (Gibco) supplemented with 10% (v/v) fetal bovine serum (FBS) and 1% (v/v) penicillin/streptomycin (Pen/Strep; 100 U mL⁻¹/100 μ g mL⁻¹) at 37°C with 5% CO₂. Cells were detached from culture flasks by trypsinization and centrifuged and resuspended. Cell number and viability were assessed with the trypan-blue dye exclusion test. Before cell seeding, sterilized scaffolds were **preincubated** overnight with standard cell culture medium (1.5 mL). Then, the scaffolds were replaced in a 24-well plate and each one was seeded by carefully dropping 30 μ L of cell suspension containing 5.0×10^4 cells onto the upper surface, allowing cell attachment for 30 min at 37°C with 5% CO₂ before adding 1.5 mL of cell culture medium. For the experiments, MSCs were incubated in osteogenic medium consisting of α -minimum essential medium supplemented with 10% (v/v) FBS, 1% (v/v) Pen/Strep, 10 mM β -glycerophosphate, 50 μ g/mL L-ascorbic acid, and 100 nM dexamethasone under standard conditions (37°C, 5% CO₂) for up to 28 days (time points: 1, 3, 7, 14, 21, and 28 days). Culture medium was partially changed every 3 days. All the cell handling procedures were performed in a sterile laminar flow hood.

Cell viability and proliferation

Cell viability was qualitatively assessed after 1 day with the LIVE/DEAD Assay Kit (Invitrogen) according to the manufacturer's instructions. This assay is based on the simultaneous determination of live and dead cells with two probes, calcein acetoxymethyl (calcein AM) and ethidium homodimer-1 (EthD-1), measuring recognized parameters of cell viability, intracellular esterase activity, and plasma membrane integrity, respectively. One sample per group was analyzed.

Cell viability and proliferation were also quantitatively assessed using MTT [3-(4,5-dimethylthiazol-2-yl)-2,5-diphenyl-tetrazolium bromide] assay. Briefly, cell/scaffold constructs were incubated with 150 μ L of MTT solution for 2 h at 37°C. In this assay, the metabolically active cells react with the tetrazolium salt in the MTT reagent to produce a formazan dye. Then, scaffolds were transferred to a tube containing 1 mL of dimethyl sulfoxide (DMSO) that dissolved formazan crystals. Two hundred microliters of supernatant was transferred to a 96-well plate and the absorbance was read at 570 nm using a Multiskan FC Microplate Photometer (Thermo Scientific). Three samples per group were analyzed at each time point. This absorbance is directly proportional to the number of metabolically active cells.

Cell-material interaction

After 1 and 7 days, one sample per group was processed for the assessment of cell adhesion using SEM. The samples



◀ AU8

◀ AU9

were washed with 0.1 M sodium cacodylate buffer, fixed in 2.5% glutaraldehyde in 0.1 M sodium cacodylate buffer for 2 h at 4°C, washed again in 0.1 M sodium cacodylate buffer, and freeze-dried. Samples were fixed on aluminum stubs using a carbon tape, sputtered with a 20-nm-thick gold layer, and analyzed using SEM (ESEM FEI Quanta 200).

Cell migration

After 14 days of cell culture, two samples per condition were collected and fixed in 4% (w/v) paraformaldehyde (PFA). After cell permeabilization with 0.1% (v/v) Triton X-100, samples were incubated with DAPI 300 nM (Invitrogen) for 7 min and washed with PBS. Scaffolds were cut longitudinally and cell migration from top to the bottom of the scaffold was analyzed with an inverted Ti-E fluorescence microscope (Nikon). The number of cells in the upper surface and in three different inner areas (top, middle, and bottom) of each scaffold composition was quantified with ImageJ software. Three representative images were evaluated for each area.

Quantitative real-time polymerase chain reaction

The gene expression profile of MSCs cultured on the three different scaffold compositions was assessed using quantitative real-time polymerase chain reaction (qPCR). The RCP scaffold was used as a calibrator to obtain a relative quantification. After 14 and 28 days of cell culture, total RNA was harvested using Tri Reagent, followed by the Direct-zol RNA MiniPrep kit (Zymo Research) according to the manufacturer's instructions. RNA integrity was analyzed by native agarose gel electrophoresis and its quantification was performed by the Qubit[®] 2.0 Fluorometer together with the Qubit RNA BR assay kit, following the manufacturer's instructions (Invitrogen). Total RNA (500 ng) was reverse transcribed to complementary DNA (cDNA) using the High-Capacity cDNA Reverse Transcription Kit, according to the manufacturer's instructions (Applied Biosystems). Relative quantification of the expression of gene alkaline phosphatase (ALP, Mm00475834), collagen I (COL1, Mm00483888_m1), osteopontin (OPN, Mm004336767), runt-related transcription factor 2 (RUNX2, Mm 00501580), and glyceraldehyde-3-phosphate dehydrogenase (GAPDH, Mm99999915_g1), used as housekeeping gene, was performed by StepOne Real-Time PCR System (Applied Biosystems). Data were collected using the OneStep software (v.2.2.2) and relative quantification was performed using the comparative threshold (C_T) method ($\Delta\Delta C_T$) where relative gene expression level equals $2^{-\Delta\Delta C_T}$. Three scaffolds per group were analyzed in three technical replicates; error bars reflect one standard error of the mean of three technical replicates as described elsewhere.^{27,28}

Western blot analysis

After 14 and 28 days, the cells were lysed in the radioimmunoprecipitation (RIPA) buffer supplemented with proteinase inhibitor cocktail (Cell Signaling). Protein concentration in each cell lysate supernatant was determined by a colorimetric assay (Kit DC Protein Assay; Bio-Rad). The protein samples were diluted in sample buffer (3:1), loaded, and separated in 4–20% Mini-PROTEAN TGX stain-free

protein gels (Bio-Rad), using a Mini-PROTEAN electrophoresis cell kit (Bio-Rad).

The proteins were then transferred to nitrocellulose membranes by means of a Trans-Blot Turbo™ transfer system (Bio-Rad), with the blots incubated thereafter for 30 min at room temperature in a blocking solution of 5% nonfat dry milk in PBS. The membranes were incubated overnight at 4°C with primary rabbit antibodies anti- β -catenin (Abcam) and anti- β -actin (Cell Signaling) as internal control, and then incubated with a horseradish goat peroxidase-linked secondary antibody anti-rabbit (Bio-Rad) for 30 min. An enhanced chemiluminescence kit (ECL; Bio-Rad) was used to visualize the protein bands with ChemiDoc XRS+ (Bio-Rad). To evaluate the relative protein expression, the β -catenin band intensities were quantified by densitometry using ImageLab software and were then normalized over the signal of the corresponding bands of β -actin (loading control).

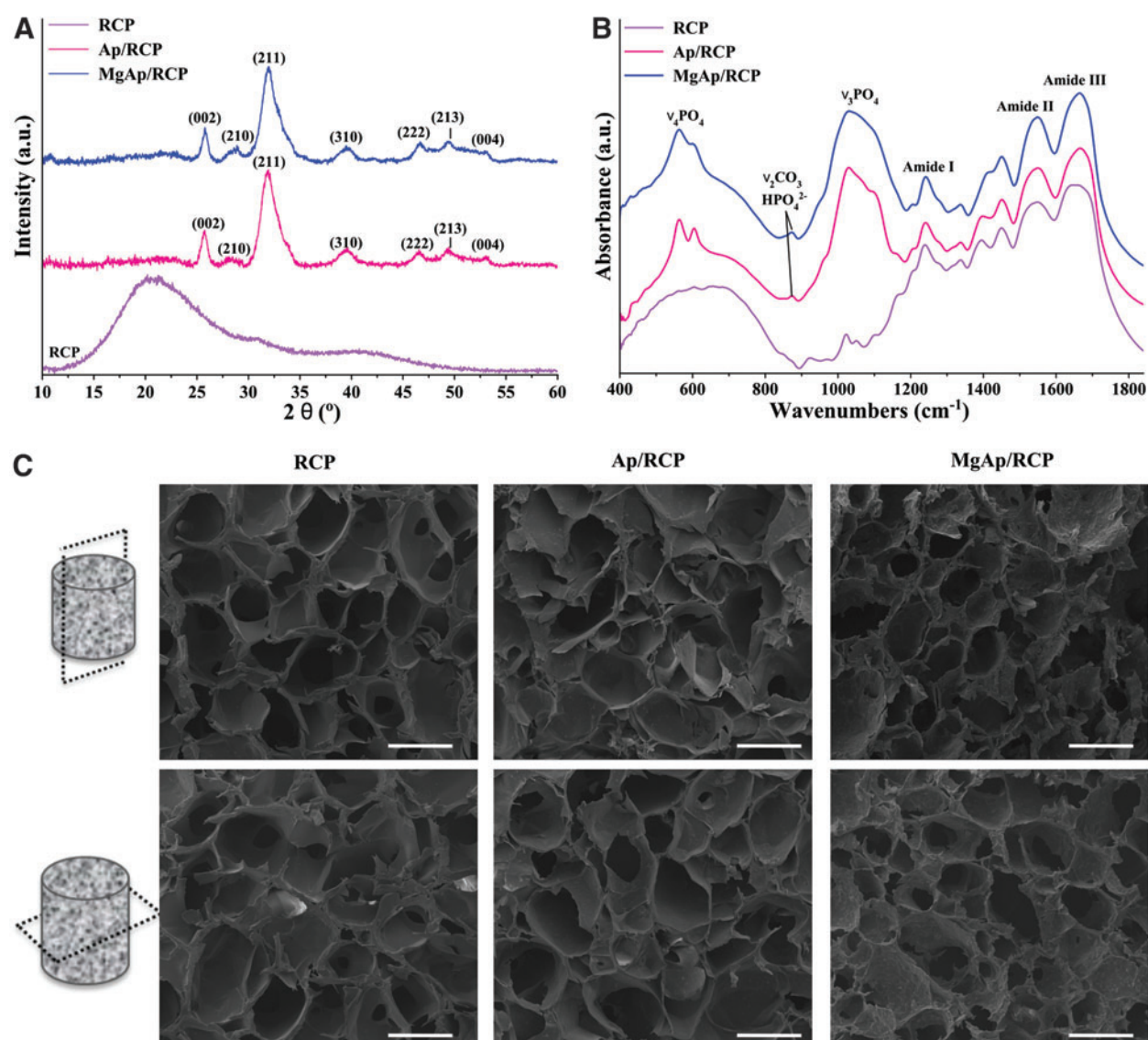
Statistical analyses

Results are expressed as average \pm SEM. Data analysis was made by two-way analysis of variance, followed by Bonferroni's *post hoc* test. Statistical analyses were performed by the GraphPad Prism software (version 6.0), with statistical significance set at $p < 0.05$.

Results

Characterization of physicochemical properties of designed 3D scaffold

The XRD pattern of **nonmineralized** (RCP) exhibited a broad band that belongs to organic phase, whereas the XRD pattern of mineralized scaffolds (Ap/RCP and MgAp/RCP) showed reflections ascribed to HA (ASTM card file No. 9-432) (Fig. 1A). The peaks were rather broad in both patterns indicating low crystallinity and nanosized dimensions of the diffracting crystal domains obtained through RCP biomimetic mineralization. In fact, FTIR spectrum of MgAp/RCP scaffolds (Fig. 1B) also exhibited broad and relatively featureless phosphate bands indicating lower crystallinity of the mineral phase compared to Ap/RCP scaffold due to the incorporation of magnesium ions that destabilizes the apatite lattice.²⁹ This effect is more clearly identified by the index for crystallinity degree calculated from FTIR spectra (splitting factor, Table 1).³⁰ All FTIR spectra showed the presence of amide bands belongs to RCP: amide I (1637 cm^{-1}), amide II (1542 cm^{-1}), and amide III (1242 cm^{-1}).³¹ FTIR spectra of mineralized scaffolds also showed the ν_2 vibration mode of CO_3^{2-} group at 873 cm^{-1} that corresponds with B-type carbonation (substitution of PO_4 by CO_3).³² The absence of the peak at 880 cm^{-1} (associated with A-type carbonation) could indicate that the carbonation can be assigned only to the B position. In fact, previous works on the synthesis of magnesium-doped apatite through the same protocol revealed the B-type carbonation that was associated with the carbon dioxide surrounding the reaction vessel.^{12,33} The presence of CO_3^{2-} ions in mineralized scaffolds may also be due to the presence of CaCO_3 impurities in the reactants. The carbonation of the as-synthesized apatite explained the fact that the Ca/P ratio of mineral phase was higher than stoichiometric hydroxyapatite (Ca/P > 1.67) (Table 1). The Mg/Ca molar ratio of MgAp/RCP scaffolds reached 1.29 wt. % with respect



AU20 ▶ **FIG. 1.** XRD (A) and FTIR (B) spectra of RCP, Ap/RCP, and MgAp/RCP scaffolds; (C) scanning electron microscopy micrographs of longitudinal and transversal section of RCP, Ap/RCP, and MgAp/RCP scaffolds. Scale bar = 250 μm . FTIR, Fourier transform infrared; RCP, recombinant collagen type I-derived peptide; XRD, X-ray diffraction. Color images available online at www.liebertpub.com/tea

to the total scaffold weight (Table 1), which was similar than the magnesium content reported for biological bone apatite.²³

With respect to scaffold microstructure, SEM observations clearly showed homogeneous pore structures in all the three scaffold compositions (Fig. 1C). Large spherical pores

were evenly distributed and well stacked along the longitudinal and transversal section. Moreover, small pores could be seen on the walls of the large ones indicating good interconnectivity. The scaffolds exhibited a mean pore size close to 250 μm in all the cases (Table 2). On the contrary, ◀T2

AU19 ▶

TABLE 1. CHEMICAL COMPOSITION OF MINERALIZED SCAFFOLDS ANALYZED BY INDUCTIVELY COUPLED PLASMA OPTICAL EMISSION SPECTROMETRY AND SPLITTING FACTOR CALCULATED FROM FOURIER TRANSFORM INFRARED SPECTRA OF MINERALIZED SCAFFOLDS

Sample	Ca (mol)	P (mol)	Ca/P (mol)	Mg (wt. %)	Mg/Ca (% mol)	SF
RCP	0.01 ± 0.01	0.00 ± 0.00	—	—	—	—
Ap/RCP	0.39 ± 0.01	0.21 ± 0.00	1.83 ± 0.04	0.10 ± 0.02	—	2.37 ± 0.04
MgAp/RCP	0.37 ± 0.00	0.20 ± 0.00	1.87 ± 0.01	1.29 ± 0.00	14.4 ± 0.06	2.09 ± 0.03

Data are expressed as average ± SEM of three samples ($n=3$).

RCP, recombinant collagen type I-derived peptide; SEM, standard error of the mean; SF, splitting factor.

TABLE 2. MACROSCOPIC SCAFFOLD PROPERTIES: MEAN PORE SIZE OF DRIED SCAFFOLDS CALCULATED FROM SCANNING ELECTRON MICROSCOPY IMAGES ($N=60$), POROSITY CALCULATED BY GRAVIMETRY METHOD ($N=5$), AND PERMEABILITY DETERMINED BY HEAD FALLING METHOD ($N=5$)

Sample	Mean pore size (μm)	Porosity (%)	Permeability 10^{-6} (m^2)
RCP	260 \pm 8	92.2 \pm 0.2	7.25 \pm 0.51
Ap/RCP	226 \pm 6	86.5 \pm 0.3	4.01 \pm 0.29
MgAp/RCP	242 \pm 7	83.3 \pm 0.2	7.91 \pm 0.54

Data are expressed as average \pm SEM.

mineralized scaffolds (Ap/RCP and MgAp/RCP) exhibited lower porosity ($\approx 86\%$ and 83% , respectively) when compared to nonmineralized one ($\approx 92\%$) (Table 2). This effect is associated with an increase of the solid loading (e.g., concentration of the nanoparticles) that promotes a decrease of the resulting scaffold porosity.³⁴ Scaffold permeability was evaluated by the falling head method. RCP and MgAp/RCP scaffolds showed similar permeability ($7 \cdot 10^{-6} \text{ m}^2$), whereas it decreased up to $4 \cdot 10^{-6} \text{ m}^2$ for Ap/RCP scaffolds (Table 2).

Evaluation of in vitro degradation of the scaffolds

The *in vitro* degradation of the scaffold was evaluated by quantification of the mass loss as well as the ion and RCP release from the scaffold under physiological condition (Fig. 2). The weight of RCP and Ap/RCP scaffolds remained nearly constant along 28 days, whereas the weight of MgAp/RCP scaffolds slightly decreased after 28 days in PBS (Fig. 2A). Moreover, ion release quantified by ICP-OES analysis indicated that MgAp/RCP scaffolds showed a faster ion release than Ap/RCP scaffolds (Fig. 2B). In fact,

Ca ion released from MgAp/RCP scaffolds was three times higher than Ca ion released from Ap/RCP scaffolds. Moreover, Ca ion release from Ap/RCP scaffolds seemed to reach a plateau after 28 days of soaking, while Ca and Mg ion release from MgAp/RCP was still rising at this time point. Surprisingly, MgAp/RCP scaffolds showed a higher cumulative Mg ion release ($7.06 \pm 0.07 \text{ wt. } \%$) compared to Ca ion ($0.16 \pm 0.01 \text{ wt. } \%$) after 28 days (Fig. 2B), indicating a faster release of Mg ions compared to Ca ions. Figure 2C displays the RCP release (wt. %) with respect to the time for the three groups. MgAp/RCP scaffolds exhibited the highest RCP release, whereas RCP scaffolds showed the lowest one. RCP release showed a similar trend than total weight loss of the scaffolds, indicating that the degradation of the scaffolds (Fig. 2A) was mainly due to the RCP release.

Cell viability and proliferation

Cell viability was qualitatively assessed after 1 day of cell culture with live/dead assay. Figure 3A shows just a few dead cells and homogeneous distribution of live cell on top of RCP, Ap/RCP, and MgAp/RCP scaffolds, indicating good cell seeding and high cell viability after 1 day of cell culture. Moreover, cell viability on the three different scaffold compositions was quantitatively assessed by MTT assay (Fig. 3B). The results indicated a significant increase of MSC proliferation over the time for all the scaffolds ($p < 0.001$). The rate of MSC proliferation on RCP and MgAp/RCP scaffolds was significantly higher than Ap/RCP scaffolds on day 3, 7, and 21 ($p < 0.01$). In detail, MgAp/RCP scaffolds showed the highest MSC proliferation at day 7, 14, and 21 of cell culture ($p < 0.01$). After 28 days of culture, these differences on MSC proliferation disappeared (Fig. 3B).

Cell-material interaction

MSC adhesion and spreading on the different scaffold compositions after 7 days of culture were analyzed by SEM

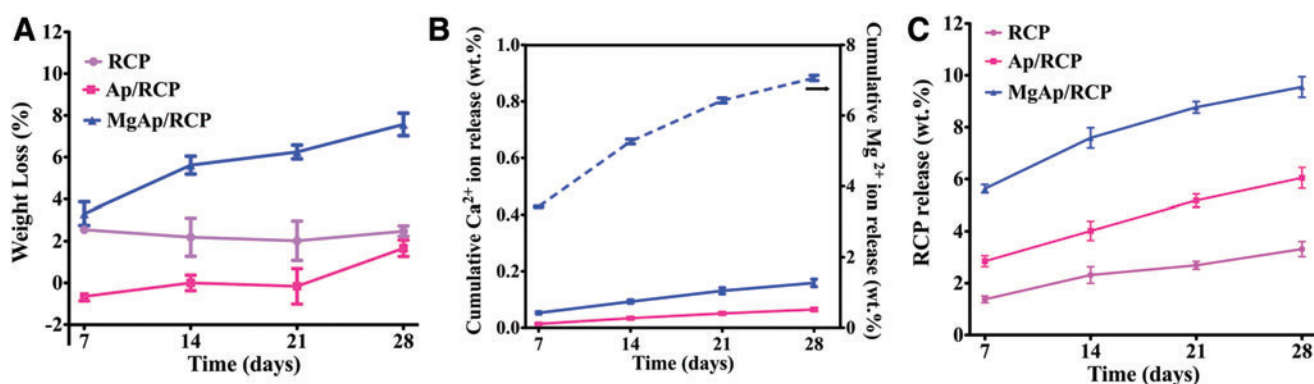


FIG. 2. *In vitro* degradation studies. (A) Degradation profile of scaffolds after soaking in PBS displayed as total weight loss of the scaffolds at each time point. (B) Cumulative ion released from Ap/RCP (pink line) and MgAp/RCP (blue line) scaffolds to PBS medium determined by ICP-OES as a function of time. Ca²⁺ ion release (wt. % with respect to the total Ca content in Ap/RCP and MgAp/RCP scaffold) is represented in continuous line (y left axis), whereas Mg²⁺ ion release (wt. % with respect to total Mg content in MgAp/RCP scaffold) is displayed in dashed line (y right axis). (C) Cumulative RCP release (wt. % with respect to total weight of the scaffold) from RCP, Ap/RCP, and MgAp/RCP scaffolds to PBS medium at different time points. Data are expressed as average \pm SEM ($n=3$). ICP-OES, inductively coupled plasma optical emission spectrometry; PBS, phosphate-buffered saline; SEM, standard error of the mean. Color images available online at www.liebertpub.com/tea

BIOMINERALIZED RCP SCAFFOLD ENHANCES MSC DIFFERENTIATION

7

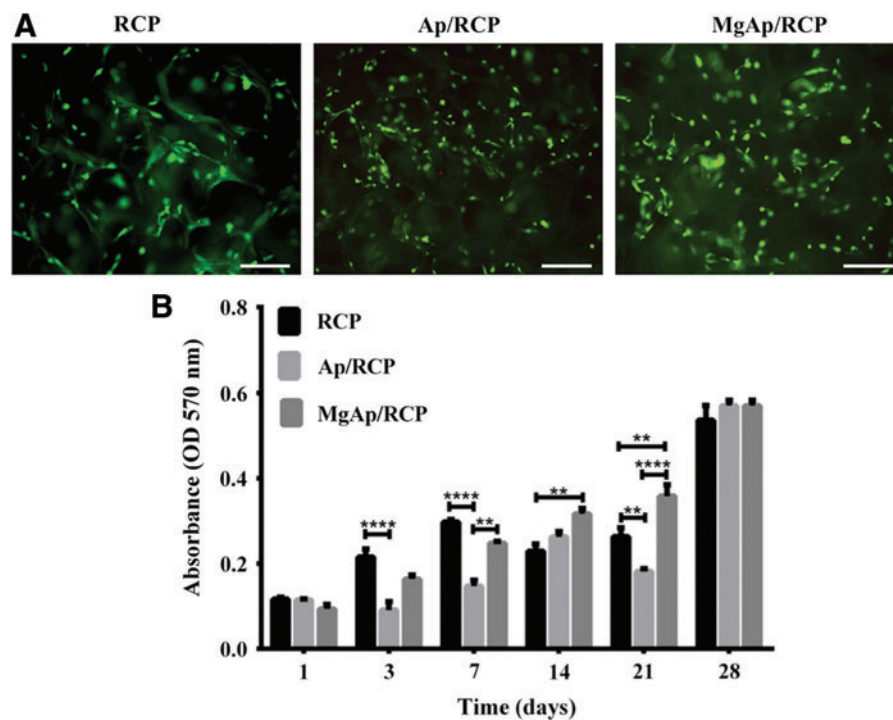


FIG. 3. Cytocompatibility. (A) Live/dead assay to evaluate cell viability after 1 day of cell culture. Live cells in *green* and dead cells in *red* on RCP, Ap/RCP, and MgAp/RCP scaffolds (scale bar: 100 μ m). (B) Cell viability evaluated by MTT assay after 1, 3, 7, 14, 21, and 28 days. Data are expressed as average \pm SEM ($n=3$). ** $p < 0.01$ and **** $p < 0.0001$. MTT, 3-(4,5-dimethylthiazol-2-yl)-2,5-diphenyltetrazolium bromide. Color images available online at www.liebertpub.com/tea

F4 ► (Fig. 4D–F). MSCs were well spread on top of the scaffold surface with tight interactions, without significant differences among the three groups.

Cell migration

While previous analyses gave an estimation of the cell proliferation over the time (MTT assay) and cell–material interaction at the top surface of the scaffolds (SEM analysis), they did not provide information related to the spatial distribution of the cells inside the scaffolds. For that purpose, each sample was longitudinally sectioned, cell nuclei were stained with DAPI, and the inner scaffold surface was scanned in three different areas (top, middle, and bottom)

F5 ► (Fig. 5B). Images of the upper surface of the scaffold (Fig. 5A) clearly revealed a larger number of cells (Fig. 5C) compared to the three different inner areas (Fig. 5D). Furthermore, MgAp/RCP scaffolds showed a larger number of cells in the inner part of the scaffold (top, middle, and bottom) compared to Ap/RCP ($p < 0.001$) and RCP scaffolds ($p < 0.0001$), as indicated in Figure 5D.

Effect of the scaffold on the osteogenic marker expression

To examine any effect on the expression of the osteogenic markers, induced by the three different scaffolds, **ascribable to the three types of scaffolds**, messenger RNA (mRNA) level of **ALP**, **RUNX2**, **OPN**, and **Col1** was analyzed by qPCR (Fig. 6) as well as **β -catenin** protein expression by western blotting (Fig. 7). The results indicated that the **ALP** expression (Fig. 6A) was **upregulated** in MSCs grown in Ap/RCP and MgAp/RCP and these differences were statistically significant compared to RCP ($p < 0.001$) after 14 days of culture. The **ALP** mRNA level decreased after 28 days of cell culture compared to 14 days. However, the significant

F6 ►

F7 ►

upregulation of this gene compared to the RCP was maintained ($p < 0.05$). The same trend was observed in **OPN** expression (Fig. 6D); in fact, MSCs cultured for 14 days on Ap/RCP and MgAp/RCP scaffolds displayed a significant increase of **OPN** mRNA level compared to RCP scaffolds ($p < 0.05$ and $p < 0.01$, respectively). The level of this gene remained unvaried after 28 days in the cells growing on Ap/RCP scaffolds, while it showed a significant **upregulation** in cells cultured in MgAp/RCP scaffolds compared to RCP and Ap/RCP ones ($p < 0.0001$). No differences were found in the **RUNX2** (Fig. 6B) and **Col1** (Fig. 6C) expression of MSCs cultured in RCP, Ap/RCP, and MgAp/RCP scaffolds at both time points.

Western blot analysis demonstrated that MSCs cultured for 28 days on MgAp/RCP scaffolds induced significantly higher expression of **β -catenin** levels (Fig. 7A) compared to MSCs cultured on RCP and Ap/RCP scaffolds ($p < 0.01$ and $p < 0.05$, respectively; Fig. 7B). Nonetheless, no statistical significant differences on **β -catenin** expression levels were found after 14 days of cell culture (Fig. 7B).

Discussion

In bone tissue regeneration, the interactions of bone substitutes with the host tissue play a key role in the regeneration process. In detail, its surface could enhance cell adhesion and/or osteogenic differentiation and often lead to an improvement of transplantation efficiency.³⁵ Current challenges in bone tissue regeneration include the engineering of scaffolds with new levels of biofunctionality that attempt to recreate nanoscale topographical and biofactor cues from bone ECM. In this work, hybrid scaffolds for bone regeneration were produced by bioinspired mineralization of RCP synergistically combining the biofunctionality provided by cell binding sites (RGD sequences) incorporated in RCP sequence, with the

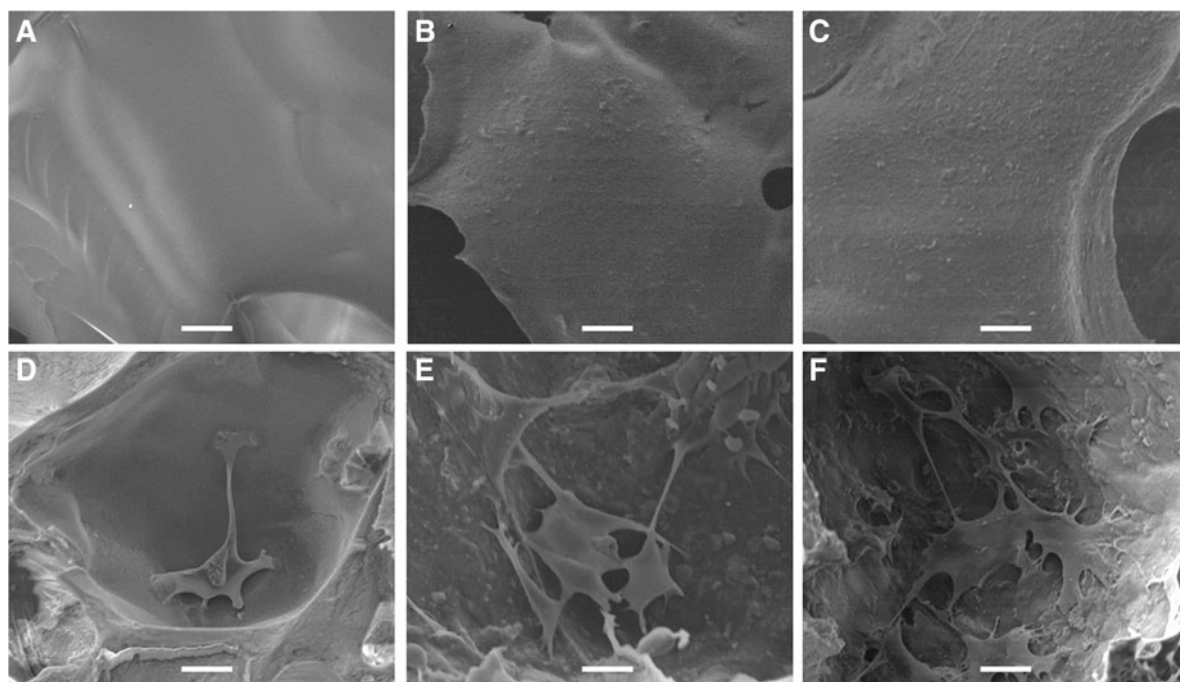
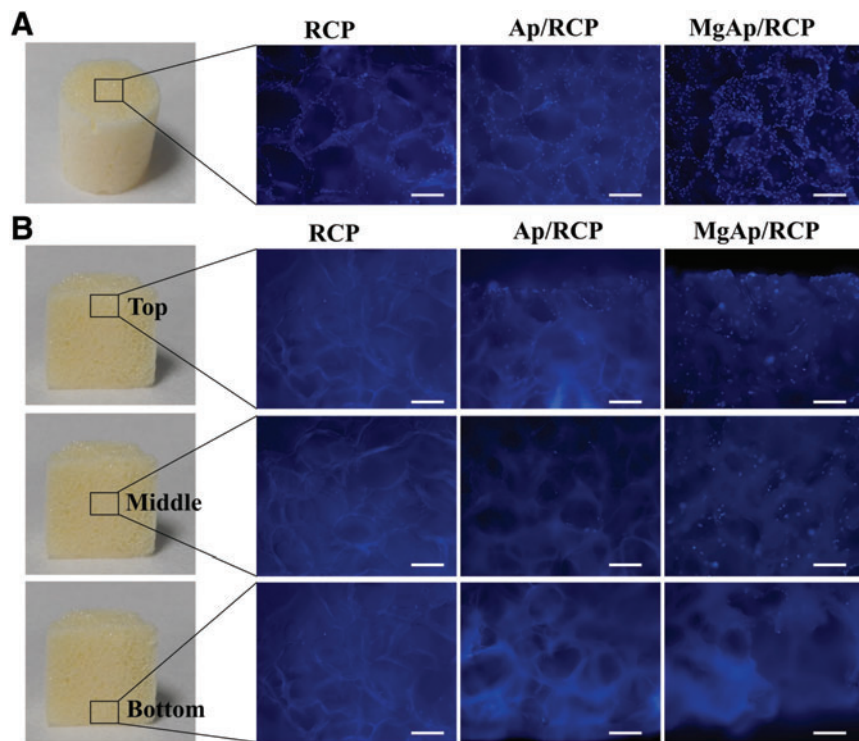
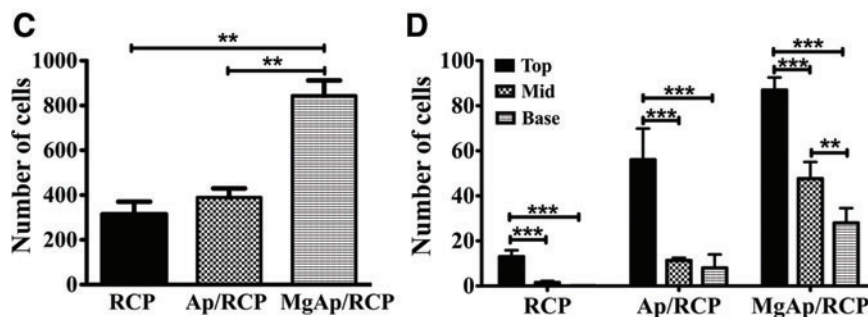


FIG. 4. Scanning electron microscopy images of the surface of RCP, Ap/RCP, and MgAp/RCP scaffolds without cells (A–C), respectively, and with MSCs adhered on the top after 7 days of cell culture (D–F), respectively. Scale bar: 20 μm. MSCs, mesenchymal stem cells.



AU21 ▶ **FIG. 5.** Cell distribution in the scaffolds after 14 days of cell culture. (A) Microscopic images of the upper surface of the scaffolds. (B) Microscopic images of three areas from inner part of scaffolds (*top*, *middle*, and *bottom*). *Blue*: cell nuclei. Scale bar: 200 μm. Graphs display the quantification of the number of cells at the upper surface of the scaffolds (C) and in three different inner areas of each scaffold (D). Data are expressed as average number of cells ± SEM obtained from three different images ($n=3$). $**p < 0.01$ and $****p < 0.0001$. Color images available online at www.liebertpub.com/tea



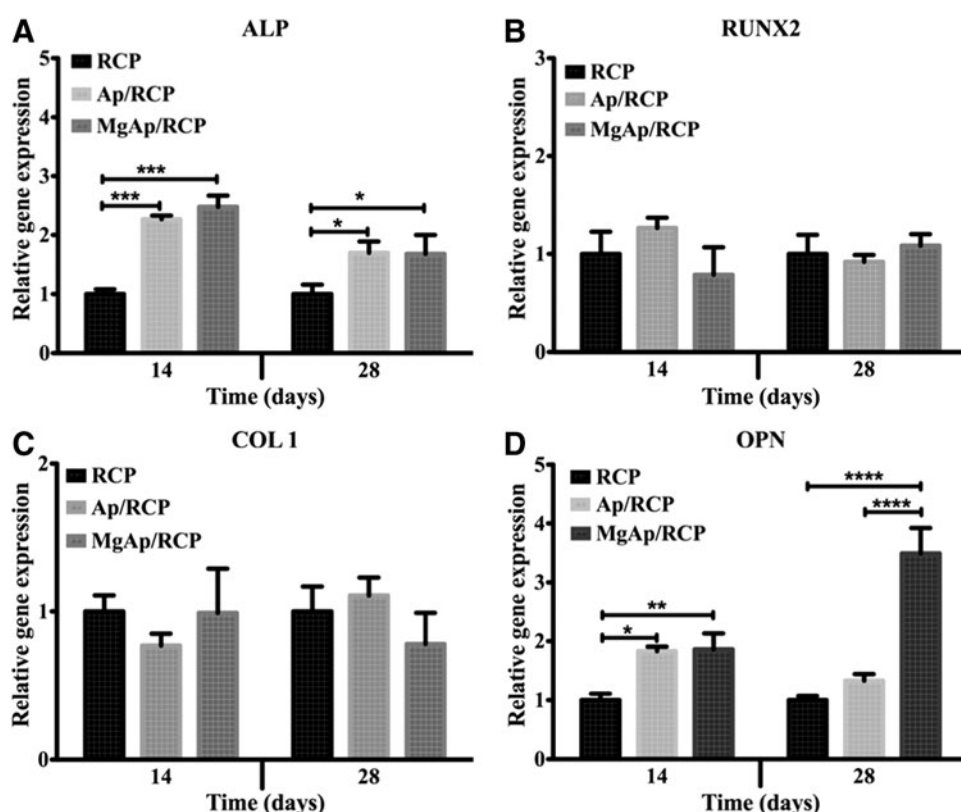


FIG. 6. Relative quantification ($2^{-\Delta\Delta C_t}$) of gene expression profiling after 14 and 28 days. Mean and standard error of the mean ($n=3$) of **ALP** (A), **RUNX2** (B), **COL1** (C), and **OPN** (D) with respect to the expression of cells grown on RCP, used as control. * $p < 0.05$, ** $p < 0.01$, *** $p < 0.001$, and **** $p < 0.0001$. **ALP**, alkaline phosphatase; **COL1**, collagen I; **OPN**, osteopontin; **RUNX2**, runt-related transcription factor 2.

◀ AU22

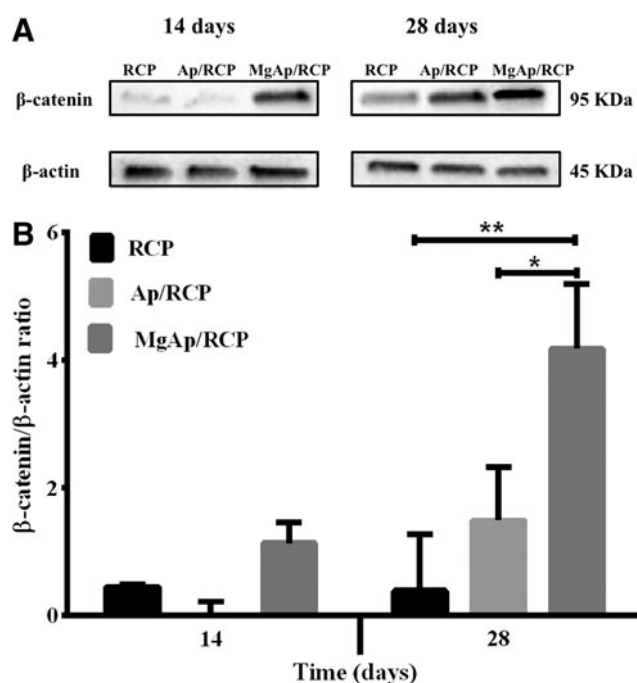


FIG. 7. Representative western blots (A) are shown with densitometry (B) of **β-catenin** expression in comparison with **β-actin** (loaded as a control) after 14 and 28 days of cell culture. Data are expressed as average \pm SEM ($n=3$). * $p < 0.05$ and ** $p < 0.01$.

bioactivity conferred by incorporation of bone-like apatite through biomimetic mineralization. The main goal is to demonstrate that biomimetalized samples enhance cell migration throughout the whole scaffold as well as potentially induce the expression of MSC osteogenic markers *in vitro*.

By monitoring the freeze-drying, 3D isotropic porous scaffolds of three different compositions were developed. The **nonmineralized** (RCP) as well as the mineralized scaffolds of magnesium showed a mean pore diameter close to 250 μm , which is on the range of pore sizes (between 200 and 350 μm) claimed as the optimum for osteoconduction.³⁶ Moreover, the porosity of designed scaffolds showed similar values to that found in cancellous bone (around 75–95%) providing the required space for marrow and blood vessel development necessary for bone regeneration.³⁷ Another key factor, correlated to porosity, to consider in the design of tissue-engineered scaffolds is the permeability that dictates diffusive transport of cytokines, nutrients, and waste throughout the scaffold.³⁸ The permeability of bone-like scaffolds designed in this work was higher than the permeability values reported for cancellous bone based on Darcy's Law,³⁹ indicating a promising *in vivo* performance of the herein designed scaffolds.

As we mentioned above, the main benefit of biomimetic mineralization protocol consists in controlling both biophysical (i.e., topography and wettability) and biochemical cues at scaffold interface that synergistically regulate the fate of MSCs in an *in vitro* or *in vivo* environment.^{40,41} Poor crystalline apatites were obtained via biomimetic mineralization of RCP as indicated by the XRD pattern. The splitting factor calculated from FTIR spectra indicated lower

crystallinity for the mineral phase contained in MgAp/RCP scaffolds compared to Ap/RCP ones. Several works pointed out that the incorporation of magnesium and carbonate into apatite destabilizes the crystal lattice decreasing their crystallinity.²⁹ Our previous work on RCP biomineralization revealed a major presence of amorphous calcium phosphate due to the simultaneous action of RCP and Mg on stabilizing the precursor phase. Moreover, Mg substitution inhibited crystal growth along *c*-axis triggering to more isometric nanocrystals.¹⁹ The same effect can be expected to occur in the synthesis of MgAp/RCP scaffolds. Crystallinity as well as crystal size (smaller crystal size prompts to higher specific surface area) affects the apatite solubility. In fact, the K_{sp} and therefore the solubility of apatite depend on several parameters such as the stoichiometry (concentration of Ca^{2+} , CO_3^{2-} , and Mg^{2+}), pH, and particle size.⁴² Previous works that evaluated solubility of the mineral phase by electrokinetic studies indicated that both the Mg substitution and B-type carbonation improved the solubility of the apatite powder at the physiological pH value (7.4).⁴³ In this work, MgAp/RCP scaffolds exhibited a faster Ca ion release kinetic when compared to Ap/RCP scaffolds under physiological conditions. It has been reported that the Ca and Mg ions in culture medium enhance adhesion and stimulate osteogenic differentiation of cells.⁴¹ Yoshizawa *et al.*⁴⁴ demonstrated that **hBMSCs** proliferated faster and they produced more mineralized matrix *in vitro* due to the presence of 10 mM $MgSO_4$ in cell culture medium. Concerning Ca, it has been found that Ca concentration of 7.8 mM in cell culture medium could enhance the proliferation and the **upregulation** of osteogenic genes in human MSCs.⁴⁵ In our studies, enhanced cell growth and proliferation were found on MgAp/RCP scaffolds when compared to Ap/RCP and RCP scaffolds at day 7, 14, and 21. This effect could be attributed to the Mg ion release from the scaffolds that was more than six times higher than the release of Ca ions. Nevertheless, cell proliferation has reached the plateau for all the groups after 28 days and did not show statistical differences among them at the end of the experiment.

AU10 ►

The *in vitro* degradation kinetic of scaffolds for bone tissue regeneration is one of the important parameters in the evaluation of their biodegradability and *in vivo* performance. The ideal scaffolds should be bioresorbable and degrade under physiological environments by the surrounding tissues to allow the ultimate replacement of scaffold material with newly formed bone without the need of surgical removal. To obtain a desired and controllable biodegradation rate for practical application, the scaffold design should consider the chemical compositions, structure of bulk materials, and crosslinking of the organic matrix.⁴ In our study, the three scaffold compositions showed good stability under physiological condition. A higher degradation rate as well as higher RCP release of MgAp/RCP scaffolds could be associated with the presence of magnesium ions that strongly interacted with carboxyl groups¹⁹ of RCP sequence responsible for the crosslinking reaction during the dehydrothermal treatment.⁴⁶

In our study, it was also important to identify those scaffolds that best supported cell colonization and proliferation within the inner part of the scaffolds since it would be a requirement for successful integration *in vivo*. The *in vitro* cell culture studies revealed that biomimetic mineralization of RCP enhanced the

cell–material interaction. In fact, MgAp/RCP scaffolds potentially induced cell migration throughout the whole 3D scaffold when compared to Ap/RCP and RCP scaffolds. Most of the previous works have been focused on determining the effect of pore size on cell attachment,^{47,48} but only a small number of works have analyzed cell migration throughout the whole 3D scaffold.^{49,50} Since scaffolds exhibited similar pore size and porosity, a greater cell migration on MgAp/RCP scaffolds could be related to the physicochemical surface properties. On one hand, the presence of Mg could improve the cell–material interaction since it has been previously reported that Mg interacts with osteoblast integrins, which are responsible for cell adhesion and stability.⁵¹ On the other hand, the role of Mg during the mineralization process prompted homogeneous mineral distribution into the organic matrix and surface nanoroughness similar to that found in bone, as previously reported.¹⁹ The main concern of cell migration inside the scaffolds is related to the *in vivo* performance of the scaffolds since the cell distribution within the scaffolds has been related to the distribution of tissue subsequently formed within engineered constructs,⁵² suggesting that uniform cell seeding could establish the basis for uniform tissue generation.

Another important indicator of bioactivity is the induction of the expression of genes and proteins related to MSC osteogenic commitment, that is, on the basis of the bone regenerative process.⁵³ The differentiation process toward osteoblasts is regulated by a number of key factors and signaling pathways. **ALP** that is responsible for the mineralization of the ECM,⁵³ **OPN** the main noncollagenous protein of the mineralized matrix,⁵⁴ and **RUNX2** often referred to as the master switch of osteogenic differentiation⁵⁵ are commonly used as markers of osteogenic differentiation *in vitro*. In this work, a protein and gene expression profile of the cells grown in the three different scaffolds was analyzed. No statistical difference was observed for **RUNX2** expression probably due to the role of this gene during the early osteogenic process, where **RUNX2** acts as a transcriptional downstream activator of bone morphogenetic protein signaling, an essential stage for the synthesis of the ECM.^{56,57} Subsequently, cells produce **ALP** and a variety of noncollagenous proteins, such as **OPN**, followed by induction of ECM calcification.⁵⁸ Our results showed that **ALP** and **OPN** genes were **upregulated** in both Ap/RCP and MgAp/RCP scaffolds compared to RCP after 14 days of culture, indicating that the physicochemical features of the scaffold provided by the presence of biomimetic apatite play an important role in the regulation of MSC fate, as previously demonstrated in *in vitro* studies of hydroxyapatite nanocrystals.⁵⁹ Moreover, in MSCs cultured for 28 days on MgAp/RCP scaffolds lead to an increase of **OPN** mRNA and **β -catenin** protein expression, considered an important factor involved in the signaling pathways that promotes MSC differentiation and osteoblast activity.⁶⁰ These results highlighted the key role of interfacial properties (chemical and physical cues) of scaffolds on cell migration and the greatest potential of MgAp/RCP scaffolds inducing MSC osteogenic differentiation *in vitro*.

Conclusions

In this work, 3D hybrid scaffolds for bone regeneration were produced by bioinspired mineralization of RCP

enriched in RGD sequences. Isotropic porous scaffolds of different compositions (nonmineralized and mineralized with and without magnesium) were fabricated with suitable pore size and permeability for cell penetration and nutrient diffusion. Biomimetic mineralization triggered poor crystalline hydroxyapatite imitating bone apatite feature (e.g., composition and crystallinity), showing lower crystallinity in the mineral phase synthesized in the presence of magnesium (MgAp/RCP). In fact, MgAp/RCP scaffolds showed a faster Ca and Mg ion release to the medium compared to Ap/RCP ones, due to mineral phase feature. *In vitro* assays indicated a better cell migration in the inner areas of bioinspired mineralized scaffold as well as an excellent potential for improving the expression of osteogenic markers of MSCs. In fact, magnesium actually heightens these effects. Thus, this work indicates a promising approach for the development of high-quality bone grafts through biomimetic mineralization of synthetic engineering peptides in the presence of magnesium ions.

Acknowledgments

We acknowledge Fujifilm Manufacturing Europe BV for supplying Cellnest. This study has been supported by the EU Marie Curie Project “Bio-inspired Bone Regeneration” (BIO-INSPIRE: Grant No. 607051, FP7-PEOPLE-2013-ITN).

Disclosure Statement

No competing financial interests exist.

AU11 ► References

- Sommerfeldt, D., and Rubin, C. Biology of bone and how it orchestrates the form and function of the skeleton. *Eur Spine J* **10**, S86, 2001.
- Salgado, A.J., Coutinho, O.P., and Reis, R.L. Bone tissue engineering: state of the art and future trends. *Macromol Biosci* **4**, 743, 2004.
- Wu, S., Liu, X., Yeung, K.W., Liu, C., and Yang, X. Biomimetic porous scaffolds for bone tissue engineering. *Mater Sci Eng R* **80**, 1, 2014.
- Henkel, J., Woodruff, M.A., Epari, D.R., Steck, R., Glatt, V., Dickinson, I.C., Choong, P.F., Schuetz, M.A., and Hutmacher, D.W. Bone regeneration based on tissue engineering conceptions—a 21st century perspective. *Bone Res* **1**, 216, 2013.
- Silber, J.S., Anderson, D.G., Daffner, S.D., Brislin, B.T., Leland, J.M., Hilibrand, A.S., Vaccaro, A.R., and Albert, T.J. Donor site morbidity after anterior iliac crest bone harvest for single-level anterior cervical discectomy and fusion. *Spine* **28**, 134, 2003.
- Lanza, R., Langer, R., and Vacanti, J.P. Principles of Tissue Engineering. Academic Press, 2011.
- Langer, R., and Vacanti, J.P. Tissue engineering. *Science* **260**, 920, 1993.
- Olszta, M.J., Cheng, X., Jee, S.S., Kumar, R., Kim, Y.-Y., Kaufman, M.J., Douglas, E.P., and Gower, L.B. Bone structure and formation: a new perspective. *Mater Sci Eng R* **58**, 77, 2007.
- Sprio, S., Sandri, M., Panseri, S., and Iafisco, M. Bone substitutes based on biomineralization. In: *Bone Substitute Biomaterials*. 2014, p. 1.
- Kim, H.-W., Kim, H.-E., and Salih, V. Stimulation of osteoblast responses to biomimetic nanocomposites of gelatin-hydroxyapatite for tissue engineering scaffolds. *Biomaterials* **26**, 5221, 2005.
- Wang, H., Bongio, M., Farbod, K., Nijhuis, A.W., van den Beucken, J., Boerman, O.C., van Hest, J.C., Li, Y., Jansen, J.A., and Leeuwenburgh, S.C. Development of injectable organic/inorganic colloidal composite gels made of self-assembling gelatin nanospheres and calcium phosphate nanocrystals. *Acta Biomater* **10**, 508, 2014.
- Tampieri, A., Sandri, M., Landi, E., Pressato, D., Francioli, S., Quarto, R., and Martin, I. Design of graded biomimetic osteochondral composite scaffolds. *Biomaterials* **29**, 3539, 2008.
- Roveri, N., Falini, G., Sidoti, M.C., Tampieri, A., Landi, E., Sandri, M., and Parma, B. Biologically inspired growth of hydroxyapatite nanocrystals inside self-assembled collagen fibers. *Mater Sci Eng C* **23**, 441, 2003.
- Chesnutt, B.M., Viano, A.M., Yuan, Y., Yang, Y., Guda, T., Appleford, M.R., Ong, J.L., Haggard, W.O., and Bumgardner, J.D. Design and characterization of a novel chitosan/nanocrystalline calcium phosphate composite scaffold for bone regeneration. *J Biomed Mater Res Part A* **88**, 491, 2009.
- Pérez, C.M.R., Stephanopoulos, N., Sur, S., Lee, S.S., Newcomb, C., and Stupp, S.I. The powerful functions of peptide-based bioactive matrices for regenerative medicine. *Ann Biomed Eng* **43**, 501, 2015.
- Zhai, Y., Cui, F.Z., and Wang, Y. Formation of nano-hydroxyapatite on recombinant human-like collagen fibrils. *Curr Appl Phys* **5**, 429, 2005.
- Zhai, Y., and Cui, F. Recombinant human-like collagen directed growth of hydroxyapatite nanocrystals. *J Cryst Growth* **291**, 202, 2006.
- Wang, Y., Cui, F., Zhai, Y., Wang, X., Kong, X., and Fan, D. Investigations of the initial stage of recombinant human-like collagen mineralization. *Mater Sci Eng C* **26**, 635, 2006.
- Ramírez-Rodríguez, G.B., Delgado-López, J.M., Iafisco, M., Montesi, M., Sandri, M., Sprio, S., and Tampieri, A. Biomimetic mineralization of recombinant collagen type I derived protein to obtain hybrid matrices for bone regeneration. *J Struct Biol* **196**, 138, 2016.
- Ruoslahti, E. RGD and other recognition sequences for integrins. *Annu Rev Cell Dev Biol* **12**, 697, 1996.
- Mumcuoglu, D., de Miguel, L., Nickel, J., Van Leeuwen, J.P., Van Osch, G.J., and Kluijtmans, S.G. BMP-2 release from synthetic collagen peptide particles. *Front Bioeng Biotechnol*. ◀AU14 ◀AU15
- Parvizi, M., Plantinga, J.A., van Speuwel-Goossens, C.A., van Dongen, E.M., Kluijtmans, S.G., and Harmsen, M.C. Development of recombinant collagen-peptide-based vehicles for delivery of adipose-derived stromal cells. *J Biomed Mater Res Part A* **104**, 503, 2016.
- Gómez-Morales, J., Iafisco, M., Delgado-López, J.M., Sarda, S., and Drouet, C. Progress on the preparation of nanocrystalline apatites and surface characterization: overview of fundamental and applied aspects. *Prog Cryst Growth Ch* **59**, 1, 2013.
- Karageorgiou, V., and Kaplan, D. Porosity of 3D biomaterial scaffolds and osteogenesis. *Biomaterials* **26**, 5474, 2005.
- Porter, A., Patel, N., Brooks, R., Best, S., Rushton, N., and Bonfield, W. Effect of carbonate substitution on the ultrastructural characteristics of hydroxyapatite implants. *J Mater Sci Mater Med* **16**, 899, 2005.
- Pennella, F., Cerino, G., Massai, D., Gallo, D., Labate, G.F.D.U., Schiavi, A., Deriu, M.A., Audenino, A., and

- Morbiducci, U. A survey of methods for the evaluation of tissue engineering scaffold permeability. *Ann Biomed Eng* **41**, 2027, 2013.
27. Ivey, K.N., Muth, A., Arnold, J., King, F.W., Yeh, R.-F., Fish, J.E., Hsiao, E.C., Schwartz, R.J., Conklin, B.R., Bernstein, H.S., and Srivastava, D. MicroRNA regulation of cell lineages in mouse and human embryonic stem cells. *Cell Stem Cell* **2**, 219, 2008.
 28. Liu, H., Peng, H., Wu, Y., Zhang, C., Cai, Y., Xu, G., Li, Q., Chen, X., Ji, J., Zhang, Y., and OuYang, H.W. The promotion of bone regeneration by nanofibrous hydroxyapatite/chitosan scaffolds by effects on integrin-BMP/Smad signaling pathway in BMSCs. *Biomaterials* **34**, 4404, 2013.
 29. Sader, M.S., Lewis, K., Soares, G.A., and LeGeros, R.Z. Simultaneous incorporation of magnesium and carbonate in apatite: effect on physico-chemical properties. *Mater Res* **16**, 779, 2013.
 30. Termine, J.D., and Posner, A.S. Infra-red determination of the percentage of crystallinity in apatitic calcium phosphates. *Nature* **211**, 268, 1966.
 31. Morris, M.D., and Finney, W.F. Recent developments in Raman and infrared spectroscopy and imaging of bone tissue. *Spectroscopy* **18**, 155, 2004.
 32. Antonakos, A., Liarokapis, E., and Leventouri, T. Micro-Raman and FTIR studies of synthetic and natural apatites. *Biomaterials* **28**, 3043, 2007.
 33. Landi, E., Tampieri, A., Mattioli-Belmonte, M., Celotti, G., Sandri, M., Gigante, A., Fava, P., and Biagini, G. Biomimetic Mg- and Mg₂CO₃-substituted hydroxyapatites: synthesis characterization and in vitro behaviour. *J Eur Ceram Soc* **26**, 2593, 2006.
 34. Deville, S., and Bernard-Granger, G. Influence of surface tension, osmotic pressure and pores morphology on the densification of ice-templated ceramics. *J Eur Ceram Soc* **31**, 983, 2011.
 35. Petrie, T.A., Raynor, J.E., Reyes, C.D., Burns, K.L., Colvard, D.M., and García, A.J. The effect of integrin-specific bioactive coatings on tissue healing and implant osseointegration. *Biomaterials* **29**, 2849, 2008.
 36. Whang, K., Healy, K., Elenz, D., Nam, E., Tsai, D., Thomas, C., Nuber, G., Glorieux, F., Travers, R., and Sprague, S. Engineering bone regeneration with bioabsorbable scaffolds with novel microarchitecture. *Tissue Eng* **5**, 35, 1999.
 37. Palmer, L.C., Newcomb, C.J., Kaltz, S.R., Spoerke, E.D., and Stupp, S.I. Biomimetic systems for hydroxyapatite mineralization inspired by bone and enamel. *Chem Rev* **108**, 4754, 2008.
 38. Caliari, S.R., and Harley, B.A. The effect of anisotropic collagen-GAG scaffolds and growth factor supplementation on tendon cell recruitment, alignment, and metabolic activity. *Biomaterials* **32**, 5330, 2011.
 39. Kohles, S.S., Roberts, J.B., Upton, M.L., Wilson, C.G., Bonassar, L.J., and Schlichting, A.L. Direct perfusion measurements of cancellous bone anisotropic permeability. *J Biomech* **34**, 1197, 2001.
 - AU16 ▶ 40. Xu, K., Chen, W., Hu, Y., Shen, X., Xu, G., Ran, Q., Mu, C., Yu, Y., and Cai, K. Influence of strontium ions incorporated nanosheet-pore topographical titanium substrates on osteogenic differentiation of mesenchymal stem cells in vitro and osseointegration in vivo. *J Mater Chem B* 2016.
 41. Samavedi, S., Whittington, A.R., and Goldstein, A.S. Calcium phosphate ceramics in bone tissue engineering: a review of properties and their influence on cell behavior. *Acta Biomater* **9**, 8037, 2013.
 42. Prakash, K., Kumar, R., Ooi, C., Cheang, P., and Khor, K.A. Apparent solubility of hydroxyapatite in aqueous medium and its influence on the morphology of nanocrystallites with precipitation temperature. *Langmuir* **22**, 11002, 2006.
 43. Landi, E., Logroscino, G., Proietti, L., Tampieri, A., Sandri, M., and Sprio, S. Biomimetic Mg-substituted hydroxyapatite: from synthesis to in vivo behaviour. *J Mater Sci Mater Med* **19**, 239, 2008.
 44. Yoshizawa, S., Brown, A., Barchowsky, A., and Sfeir, C. Magnesium ion stimulation of bone marrow stromal cells enhances osteogenic activity, simulating the effect of magnesium alloy degradation. *Acta Biomater* **10**, 2834, 2014.
 45. Barradas, A.M., Fernandes, H.A., Groen, N., Chai, Y.C., Schrooten, J., van de Peppel, J., van Leeuwen, J.P., van Blitterswijk, C.A., and de Boer, J. A calcium-induced signaling cascade leading to osteogenic differentiation of human bone marrow-derived mesenchymal stromal cells. *Biomaterials* **33**, 3205, 2012.
 46. Ozeki, M., and Tabata, Y. In vivo degradability of hydrogels prepared from different gelatins by various cross-linking methods. *J Biomater Sci Polym Ed* **16**, 549, 2005.
 47. Tierney, C.M., Haugh, M.G., Liedl, J., Mulcahy, F., Hayes, B., and O'Brien, F.J. The effects of collagen concentration and crosslink density on the biological, structural and mechanical properties of collagen-GAG scaffolds for bone tissue engineering. *J Mech Behav Biomed Mater* **2**, 202, 2009.
 48. O'Brien, F.J., Harley, B.A., Yannas, I.V., and Gibson, L.J. The effect of pore size on cell adhesion in collagen-GAG scaffolds. *Biomaterials* **26**, 433, 2005.
 49. Sobral, J.M., Caridade, S.G., Sousa, R.A., Mano, J.F., and Reis, R.L. Three-dimensional plotted scaffolds with controlled pore size gradients: effect of scaffold geometry on mechanical performance and cell seeding efficiency. *Acta Biomater* **7**, 1009, 2011.
 50. Allan, I.U., Tolhurst, B.A., Shevchenko, R.V., Dainiak, M.B., Illsley, M., Ivanov, A., Jungvid, H., Galaev, I.Y., James, S.L., Mikhailovsky, S.V., and James, S.E. An in vitro evaluation of fibrinogen and gelatin containing cryogels as dermal regeneration scaffolds. *Biomater Sci* **4**, 1007, 2016.
 51. Yamasaki, Y., Yoshida, Y., Okazaki, M., Shimazu, A., Uchida, T., Kubo, T., Akagawa, Y., Hamada, Y., Takahashi, J., and Matsuura, N. Synthesis of functionally graded MgCO₃ apatite accelerating osteoblast adhesion. *J Biomed Mater Res* **62**, 99, 2002.
 52. Holy, C.E., Shoichet, M.S., and Davies, J.E. Engineering three-dimensional bone tissue in vitro using biodegradable scaffolds: investigating initial cell-seeding density and culture period. *J Biomed Mater Res* **51**, 376, 2000.
 53. Granéli, C., Thorfve, A., Ruetschi, U., Brisby, H., Thomsen, P., Lindahl, A., and Karlsson, C. Novel markers of osteogenic and adipogenic differentiation of human bone marrow stromal cells identified using a quantitative proteomics approach. *Stem Cell Res* **12**, 153, 2014.
 54. Aubin, J.E. Regulation of osteoblast formation and function. *Rev Endocr Metab Disord* **2**, 81, 2001.
 55. Deng, Z.-L., Sharff, K.A., Tang, N., Song, W.-X., Luo, J., Luo, X., Chen, J., Bennett, E., Reid, R., and Manning, D.

BIOMINERALIZED RCP SCAFFOLD ENHANCES MSC DIFFERENTIATION

13

Regulation of osteogenic differentiation during skeletal development. *Front Biosci* **13**, 2001, 2008.

56. Gersbach, C.A., Byers, B.A., Pavlath, G.K., and García, A.J. Runx2/Cbfa1 stimulates transdifferentiation of primary skeletal myoblasts into a mineralizing osteoblastic phenotype. *Exp Cell Res* **300**, 406, 2004.
57. Franceschi, R.T., Ge, C., Xiao, G., Roca, H., and Jiang, D. Transcriptional regulation of osteoblasts. *Ann N Y Acad Sci* **1116**, 196, 2007.
58. Malaval, L., Liu, F., Roche, P., and Aubin, J.E. Kinetics of osteoprogenitor proliferation and osteoblast differentiation in vitro. *J Cell Biochem* **74**, 616, 1999.
- AU17► 59. Montesi, M., Panseri, S., Iafisco, M., Adamiano, A., and Tampieri, A. Effect of hydroxyapatite nanocrystals functionalized with lactoferrin in osteogenic differentiation of mesenchymal stem cells. *J Biomed Mater Res Part A* 2014.
60. Holmen, S.L., Zylstra, C.R., Mukherjee, A., Sigler, R.E., Faugere, M.-C., Bouxsein, M.L., Deng, L., Clemens, T.L., and Williams, B.O. Essential role of β -catenin in postnatal bone acquisition. *J Biol Chem* **280**, 21162, 2005.

Address correspondence to: ◀AU18

Gloria Belén Ramírez-Rodríguez
Institute of Science and Technology for Ceramics (ISTEC)
National Research Council (CNR)
Faenza
Italy

E-mail: gloriaramirez.iq@gmail.com

Monica Montesi
Institute of Science and Technology for Ceramics (ISTEC)
National Research Council (CNR)
Faenza
Italy




E-mail: monica.montesi@istec.cnr.it

Received: January 15, 2017

Accepted: May 24, 2017

Online Publication Date:

AUTHOR QUERY FOR TEA-2017-0028-VER9-RAMIREZ-RODRIGUEZ_1P

- AU1: Please note that gene symbols in any article should be formatted as per the gene nomenclature. Thus, please make sure that gene symbols, if any in this article, are italicized.
- AU2: Please mention the degrees of all authors.
- AU3: Please review all authors' surnames for accurate indexing citations.
- AU4: Please confirm the authors' affiliation and also mention the department name for the affiliation.
- AU5: Please note that the keywords have been taken from the PDF. Please check and confirm if this is OK.
- AU6: The Publisher requests for readability that no paragraph exceeds 15 typeset lines. Please check for long paragraphs and divide where needed.
- AU7: Please note that the acronym "SEM" has been abbreviated as "scanning electron microscopy" as well as "standard error of the mean." Please check and clarify.
- AU8: Please check and confirm whether the edits made to the sentence "For the experiments, MSCs were ..." is OK.
- AU9: Please check the edits made to the sentence "The samples were washed...."
- AU10: Please expand "hBMSCs."
- AU11: Please note that Ref. 4  a duplicate of Ref. 19. Hence, Ref. 42 has been deleted and references have been renumbered accordingly. Please check.
- AU12: Please mention the publisher location for "Ref. 6."
- AU13: Please mention the editors' names, publisher name, and publisher location for "Ref. 9."
- AU14: Please mention the publication year, volume number, and page number for "Ref. 21."
- AU15: Please mention the volume number and page number for "Ref. 21."
- AU16: Please mention the volume number and page number for "Ref. 40."
- AU17: Please mention the volume number and page number for "Ref. 59."
- AU18: Please provide the complete address with postal code for the corresponding authors. Also mention the degrees for the corresponding authors.
- AU19  Please check and confirm whether "Table 1" title has been set correctly.
- AU20  Please check and confirm whether the edits made to "Figure 1" legend is OK.
- AU21: Please note that "****" is present in the artwork of "Figure 5" but not mentioned in the figure legend. Also note that "*****" is mentioned in "Figure 5" legend but not present in the artwork. Please check.
- AU22: Please note that both "COLI" and "COL1" have been used. Please fix them consistently.

EDITOR QUERY FOR TEA-2017-0028-VER9-RAMIREZ-RODRIGUEZ_1P

- EQ1: Please check the <MT> and <TYPE> of this manuscript.